Optical Characterization of Thin Colloidal Gold Films by Spectroscopic Ellipsometry

E. Stefan Kooij,* Herbert Wormeester, E. A. Martijn Brouwer,
Esther van Vroonhoven, Arend van Silfhout, and Bene Poelsema

*MESA Research Institute and Faculty of Applied Physics, University of Twente,
P.O. Box 217, 7500 AE Enschede, The Netherlands*

Spectroscopic ellipsometry and atomic force microscopy (AFM) experiments are employed to characterize nanocolloidal gold films, self-assembled at APTES-derivatized Si/SiO$_2$ surfaces. X-ray fluorescence measurements after deposition confirm that AFM provides a representative means to probe the absolute surface coverage. Optical properties of gold nanocrystal assemblies are investigated both ex situ after drying and in situ prior to evaporation of the solvent. Quantitative optical characterization of these highly inhomogeneous systems is not unambiquous. Conventional effective medium approximations are not applicable to these systems. To enable an accurate analysis, extinction measurements on colloidal suspensions are performed. The limited particle size in relation to the electron mean free path leads to a modification of the dielectric function at longer wavelengths. Ellipsometry spectra of the colloidal gold films are analyzed qualitatively using an optical invariant and principal component analyses. Quantitative results are obtained using a theory which treats the nanocrystals as polarizabilities at the Fresnel interface. Above approximately 20%, the coverages determined from optical spectra are in agreement with what is found from AFM images. At lower coverages, the optical results seem to overestimate the actual nanocrystal density. The discrepancies are discussed in terms of image charge effects arising from the proximity of the substrate.

Introduction

The unique and new optical, electrical, and magnetic properties of colloidal superstructures as opposed to the bulk characteristics of the constituent materials are attracting the attention of an increasing number of both fundamental and technology-oriented-industry scientists.[1,2] The colloid size used in the assembled structures varies over approximately 3 orders of magnitude and is closely related to the specific application. For photonic band gap materials the particle size is of the same order as the wavelength of light,[1−4] while for magnetic applications, such as ultrahigh-density storage devices, the particle radius is in the low-nanometer range.[5−7] Combination of the aforementioned physical properties of colloidal matter introduces even more exciting fields of research. Recently, for example, the magnetically tuneable spin-dependent tunneling in cobalt nanocrystal superlattices was described.[8]

A prerequisite for studying colloidal systems is the ability to characterize them unambiguously under relevant conditions. Among the large number of methods available for characterizing colloids and their superstructures, electron microscopy (SEM/TEM) is by far the most popular.[1−14] For both very small as well as relatively large particles, this is the most employed ex situ technique.

The use of scanning probe microscopy (AFM, STM, MFM) among colloid scientists is increasing, but also with this technique experiments are typically performed ex situ.[10,15] In fact, only optical methods have been employed in situ. Imaging techniques such as conventional[12,13,16] or confocal[1,17] microscopy are used for large colloids. For sizes much smaller than the wavelength of light, such as with gold nanoparticles, only nonimaging (lateral averaging) in situ experiments are available. These include primarily UV/vis absorption spectroscopy,[1,2,6,9,14,15] but also optical waveguide light mode spectroscopy,[18] and reflection techniques such as reflectometry and ellipsometry.[19−21]

The major advantage of ellipsometry as compared to reflectometry is its sensitivity to very small perturbations at an interface.[22,23] Additionally, owing to the noninvasive character, ellipsometry is a powerful in situ technique to study a large variety of surface processes,[24] such as growth nucleation[25] as well as the deposition and drying processes

(1) *MRS Bulletin*, Vol. 23; Materials Research Society: Warrendal, PA, 1998.
(2) Xia, Y.; Gates, B.; Lin, Y.; Lu, Y. *Adv. Mater.* **2000**, *12*, 693−713.
(3) van Blaaderen, A. *Science* **1998**, *282*, 887−888.
(4) Koenderink, A. F.; Megens, M.; van Soest, G.; Vos, W. L.; Lagendijk, A. *Phys. Lett. A* **2000**, *268*, 104−111.
(5) Sun, S.; Murray, C. B.; Weller, D.; Folks, L.; Moser, A. *Science* **2000**, *287*, 1989−1992.
(6) Murray, C. B.; Kagan, C. R.; Bawendi, M. G. *Annu. Rev. Mater. Sci.* **2000**, *20*, 545−610.
(7) Puntes, V. F.; Krishnan, K. M.; Alivisatos, P. *Appl. Phys. Lett.* **2001**, *78*, 2187−2189.
(8) Black, C. T.; Murray, C. B.; Sandstrom, R. L.; Sun, S. *Science* **2000**, *290*, 1131−1134.
(9) Grabar, K. C.; Freeman, R. G.; Hommer, M. B.; Natan, M. J. *Anal. Chem.* **1995**, *67*, 735−743.

(10) Grabar, K. C.; Brown, K. R.; Keating, C. D.; Stranick, S. J.; Tang, S.-L.; Natan, M. J. *Anal. Chem.* **1997**, *69*, 471−477.
(11) Giersig, M.; Mulvaney, P. *Langmuir* **1993**, *9*, 3408.
(12) Trau, M.; Saville, D. A.; Aksay, I. A. *Science* **1996**, *272*, 706−709.
(13) Böhmer, M. *Langmuir* **1996**, *12*, 5747−5750.
(14) Jana, N. R.; Gearheart, L.; Murphy, C. J. *Langmuir* **2001**, *17*, 6782−6786.
(15) Schmitt, J.; Mächtle, P.; Eck, D.; Möhwald, H.; Helm, C. A. *Langmuir* **1999**, *15*, 3256−3266.
(16) Trau, M.; Saville, D. A.; Aksay, I. A. *Langmuir* **1997**, *13*, 6375−6381.
(17) Dinsmore, A. D.; Weeks, E. R.; Prasad, V.; Levitt, A. C.; Weitz, D. A. *Appl. Opt.* **2001**, *40*, 4152−4159.
(18) Picart, C.; Ladam, G.; Senger, B.; Voegel, J.-C.; Schaaf, P.; Cuisinier, F. J. G.; Gergely, C. *J. Chem. Phys.* **2001**, *115*, 1086−1094.
(19) Böhmer, M. R.; van der Zeeuw, E. A.; Koper, G. J. M. *J. Colloid Interface Sci.* **1995**, *197*, 242−250.
(20) Baum, T.; Benthell, D.; Brust, M.; Schiffrin, D. J. *Langmuir* **1999**, *15*, 866−871.
(21) Koper, G. J. M. *Colloids Surf., A* **2000**, *165*, 39−57.
(22) Tompkins, H. G.; McGahan, W. A. *Spectroscopic ellipsometry and reflectometry: a user's guide*; John Wiley & Sons: New York, 1999.
(23) Azzam, R. M. A.; Bashara, N. H. *Ellipsometry and polarized light*; North-Holland: Amsterdam, 1987.

of (nano-) colloidal particles at a solid−liquid interface.[19−21] In two totally different research fields, spectroscopic ellipsometry has recently also proven its power in the in situ study of (i) the optical changes accompanying (de)-hydrogenation of rare earth metal hydride films[26,27] and (ii) the CO_2 sorption behavior in inorganic materials.[28]

In this paper we investigate the optical properties of colloidal gold films by means of spectroscopic ellipsometry. Gold particles are deposited from a colloidal gold suspension on silicon substrates covered with a thin layer of oxide. To enhance the affinity for the gold nanocrystals, the surface is derivatized with (3-aminopropyl)triethoxysilane (APTES). The amino end groups serve as anchor sites for the gold particles;[9,10,15] because of the strong bonding of the particles, the surface mobility is negligible and the deposition is governed by random sequential adsorption (RSA).[29] A higher degree of ordering has been achieved by electrophoretic deposition,[11,12] which was shown to be very successful with much larger particles.[13,16]

An unambiguous optical characterization of colloidal systems and assemblies is not straightforward. In this paper we present ex situ ellipsometry spectra on samples after drying as well as results of an in situ experiment after deposition but prior to drying. The ex situ spectra are compared to AFM measurements on these samples, enabling the determination of the accuracy of ellipsometry experiments. This provides a basis for evaluating the analysis strategies for optical spectra.

To enable an accurate optical analysis, we first discuss the single-particle polarizability. The agreement between measured and calculated extinction coefficients of the colloidal gold suspension can be improved substantially by using a simple modification of the effective dielectric function of bulk gold in terms of the limited electron mean free path in the nanoparticles.[30]

The ellipsometry spectra are analyzed using two different routes: (i) In a top-down approach we use an optical invariant in combination with a principal component analysis.[31] More quantitative analysis yields the dielectric function of the gold nanocrystal films, which is then compared to the single-particle polarizability. (ii) A bottom-up strategy is employed in which the ellipsometry spectra are compared to simulations using conventional effective medium approximations. We show that these cannot be used to analyze the colloidal gold films. Considerably better results are obtained with the "thin island film" theory established by Bedeaux and Vlieger.[32,33]

In both approaches the coverages determined from the ellipsometry results are in excellent agreement with what is obtained from AFM measurements for coverages above approximately 20%. However, below 20% surface coverage, the optically derived coverage overestimates that found

(24) de Nijs, J. Ellipsometry and the Ti/c-Si solid-state reaction. Ph.D. Thesis, University Twente, Enschede, 1989.

(25) Kelly, J. J.; Vondeling, J. K. *J. Electrochem. Soc.* **1975**, *122*, 1103−1107.

(26) van Gogh, A. T. M.; Nagengast, D. G.; Kooij, E. S.; Koeman, N. J.; Rector, J. H.; Griessen, R.; Flipse, C. F. J.; Smeets, R. J. J. G. A. M. *Phys. Rev. B* **2001**, *63*, 195105.

(27) Mor, G. K.; Malhotra, L. K.; Bhattacharyya, D. *J. Appl. Phys.* **2001**, *90*, 1795−1800.

(28) Benes, N. E.; Spijksma, G.; Verweij, H.; Wormeester, H.; Poelsema, B. *AIChE J.* **2001**, *47*, 1212−1218.

(29) Oberholzer, M. R.; Stankovich, J. M.; Carnie, S. L.; Chan, D. Y. C.; Lenhoff, A. M. *J. Colloid Interface Sci.* **1997**, *194*, 138−153.

(30) Kreibig, U.; Vollmer, M. *Optical properties of metal clusters*; Springer-Verlag: Berlin Heidelberg, 1995.

(31) Chatfield, C.; Collins, A. J. *Introduction to multivariate analysis*; Chapman and Hall: London, 1980.

(32) Bedeaux, D.; Vlieger, J. *Physica* **1973**, *67*, 55−77.

(33) Bedeaux, D.; Koper, G. J. M.; van der Zeeuw, E. A.; Vlieger, J.; Wind, M. M. *Physica A* **1994**, *207*, 285−292.

from topographic AFM images. This discrepancy at low coverages is discussed in terms of image charge effects arising from the interaction of the gold nanocrystals and the substrate onto which they are adsorbed.

Spectroscopic Ellipsometry on Thin Island Films

In this section we briefly review the principles of ellipsometry and the analysis method established by Abeles. Additionally, we describe possible ways to treat the optical properties of random colloidal films, such as effective medium approximations.

The complex reflection coefficient ρ obtained from ellipsometry is defined as

$$\rho \equiv \frac{r^p}{r^s} \equiv \tan \Psi \exp(i\Delta) \qquad (1)$$

where r^p and r^s are the reflection coefficients for the parallel and perpendicular polarizations, respectively.[22] For a single interface, r^p and r^s represent the Fresnel reflection coefficients. Historically, the complex quantity ρ is expressed in the two angles Ψ and Δ. The absolute value $|\rho| = |r^p/r^s|$ is represented by $\tan \Psi$, while the phase change between the two polarization directions is related to $\cos \Delta$. In fact, $\tan^2 \Psi$ is the quantity measured in polarized reflectometry. However, the analysis of the reflective properties of (very) thin layers indicates that the largest effects are in $\cos \Delta$. Although the actual ellipsometry measurement is relatively simple, the analysis of the results is often complicated.[22,23] A model is required for the system under consideration, which can then be used to simulate or fit the results.

The optical response of a multilayered structure with known dielectric functions can be simulated using the Abeles matrix algorithm. Details of the original method are described by Azzam and Bashara.[23] Two types of matrices are employed. One describes the transition from medium m to medium $m + 1$ and is defined as

$$I_{m,m+1} = \frac{1}{t_{m,m+1}}\begin{pmatrix} 1 & r_{m,m+1} \\ r_{m,m+1} & 1 \end{pmatrix} \qquad (2)$$

with $r_{m,m+1}$ and $t_{m,m+1}$ the Fresnel reflection and transmission coefficients.

Another matrix describes the light passage through the medium and involves the phase factors

$$L_m = \begin{pmatrix} e^{-i\Delta_m} & 1 \\ 1 & e^{-i\Delta_m} \end{pmatrix} \qquad (3)$$

where $\Delta_m = (2\pi/\lambda)d_m n_m \cos(\theta_m)$ with λ the wavelength of the light in a vacuum (in nanometers), d_m the thickness of layer m (in nanometers), θ_m the angle of the light, and n_m the refractive index of medium m. The angles in the various media are related through Snell's law: $n_m \sin(\theta_m) = n_{m+1} \sin(\theta_{m+1})$.

For our system consisting of a colloidal gold layer ($m = 2$) and a silicon dioxide film ($m = 3$) on a silicon substrate ($m = 4$), in contact with the ambient (air or aqueous solution; $m = 1$), a matrix product is defined

$$A = I_{1,2}L_2 I_{2,3} L_3 I_{3,4} \qquad (4)$$

and the overal reflection coefficient is calculated from $r = A_{21}/A_{11}$. For both the parallel and perpendicular polarizations, the reflection coefficients r^p and r^s can be

obtained by inserting the appropriate Fresnel coefficients in eq 2 and the ellipsometric quantity in eq 1 can be calculated.

To model ellipsometry spectra, the dielectric function of inhomogeneous media is often treated in terms of an effective medium approximation.[30] For two types of spherical inclusions (with ϵ_a and ϵ_b) in a host matrix (with ϵ_h), the effective dielectric function ϵ_{eff} is given by

$$\frac{\epsilon_{eff} - \epsilon_h}{\epsilon_{eff} + 2\epsilon_h} = f_a\frac{\epsilon_a - \epsilon_h}{\epsilon_a + 2\epsilon_h} + f_b\frac{\epsilon_b - \epsilon_h}{\epsilon_b + 2\epsilon_h} \qquad (5)$$

where f_a and f_b are the volume fractions of the materials with dielectric functions ϵ_a and ϵ_b, respectively. Replacing f_b by $1 - f_a$ and substituting $\epsilon_h = \epsilon_{eff}$ gives the effective medium approximation established by Bruggeman, while inserting $\epsilon_h = \epsilon_b$ corresponds to the Maxwell–Garnett approximation.

As we will show later, these effective medium approximations yield unsatisfactory results. Another method for treating the optical properties of particulate films is provided by the thin island film theory as originally described by Bedeaux and Vlieger.[32,33] If the constituent entities are small compared to the wavelength of the light, they can be described in terms of excess optical susceptibilities. Recently, an elaborate review has been published by G. J. M. Koper[21] and an application of the theory to a reflectometry experiment has been described by Böhmer et al.[19]

For a film of identical small spherical particles, the susceptibilities have been calculated by Haarmans and Bedeaux.[34] The optical response to an electromagnetic field is in a good approximation described in terms of polarizabilities along the surface and normal to the substrate, respectively,

$$\gamma = \frac{8\pi\epsilon_1}{\lambda}\left(\frac{\epsilon - \epsilon_1}{\epsilon + 2\epsilon_1}\right)\varphi r \qquad (6)$$

$$\beta = \frac{8\pi}{\lambda\epsilon_1}\left(\frac{\epsilon - \epsilon_1}{\epsilon + 2\epsilon_1}\right)\varphi r \qquad (7)$$

with ϵ and ϵ_1 the dielectric functions of the spheres (gold in this case) and the suspending medium (air/water), φ the surface coverage, and r the particle radius. The reflection and transmission coefficients depend on the polarization of the light and are for s-polarized light

$$r_/^s = \frac{X^s}{1 - X^s}$$

and

$$t_/^s = \frac{1}{1 - X^s}$$

with

$$X^s = \frac{i\gamma}{2n_1 \cos(\theta_1)}$$

and for p-polarized light

(34) Haarmans, M. T.; Bedeaux, D. *Thin Solid Films* **1995**, *258*, 213–223.

$$r_/^p = \frac{X^p}{1 - X^p} - \frac{Y^p}{1 - Y^p}$$

and

$$t_/^p = 1 + \frac{X^p + Y^p - 2X^p Y^p}{(1 - X^p)(1 - Y^p)}$$

with

$$X^p = \frac{i\beta(n_1)^3 \sin^2(\theta_1)}{2 \cos(\theta_1)}$$

and

$$Y^p = \frac{i\gamma \cos(\theta_1)}{2n_1}$$

The Abeles film matrix for such a particulate film in terms of these reflection and transmission coefficients is given by

$$F = \frac{1}{t_/}\begin{pmatrix} 1 & -r_/ \\ r_/ & t_/^2 - r_/^2 \end{pmatrix} \qquad (8)$$

and for our system the modified overal matrix becomes

$$A' = FL_F I_{1,3} L_3 I_{3,4} \qquad (9)$$

The layer matrix L_F is identical to L_m in eq 3, but with a phase factor $\Delta = (2\pi/\lambda)hn_1 \cos\theta_1$, where h is the height of the excess susceptibilities above the Fresnel interface. Often, the distance $h = r$ between the bare substrate and the particle centers is used. Note that the film matrix F is different from the interface matrix $I_{m,m+1}$, as for an interface $r_{m,m+1} = -r_{m+1,m}$, which is obviously not true for the reflection coefficients $r_/^s$ and $r_/^p$ of a thin film.

Experimental Details

Materials. All chemicals are used as received, without any further purification. Sodium citrate (99%) and hydrogen tetrachloroaurate (HAuCl$_4$, 99.999%) are obtained from Aldrich; all other chemicals are "for analysis" grade from Merck. Aqueous solutions are prepared with water purified in a Milli-Q system.

Colloid Preparation. Colloidal gold suspension are prepared by standard citrate reduction.[9,35] Typically, 100 mL of 1 mM HAuCl$_4$ aqueous solution is heated to 100 °C under refluxing conditions. While stirring vigorously, 10 mL of 38.8 mM sodium citrate is quickly added, resulting in color changes of the originally yellow solution to transparent, to dark blue/gray, and, finally, after approximately 2 min, to burgundy red, which marks the end of the reaction. The mixture is kept at 100 °C for 15 min and subsequently cooled to room temperature with continuous stirring.

The particle size has been determined by three different methods. (HR)TEM measurements show that the gold particles are spherical multidomain crystallites with a diameter of 12.8 nm; the size dispersion amounts to $\sigma = 8$–10%. Second, the average height of particles in AFM images amounts to 13.2 nm; laterally, the size of the particles is overestimated because of tip-convolution. Finally, X-ray fluorenscence measurements are performed to determine the number of gold atoms on the surface. In Figure 1 this is compared to the number density of gold particles obtained from AFM images on the same samples. The linear relation indicates that the average number of gold atoms per nanocrystal amounts to 7.62×10^4; using the bulk density of gold (19.32 g/cm^3), this results in the particle diameter 13.5 nm.

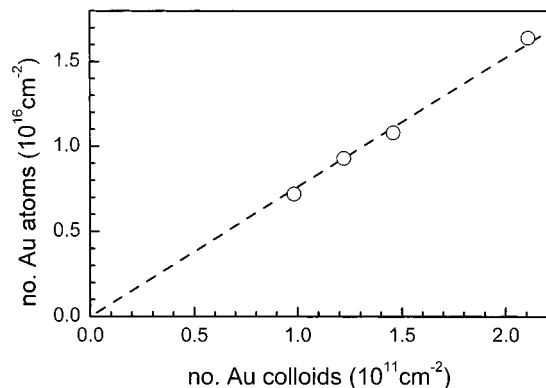(35) Frens, G. *Nat. Phys. Sci.* **1973**, *241*, 20–22.

Figure 1. Surface density of gold atoms determined from X-ray fluorescence spectroscopy, as a function of the gold nanocrystal density, obtained by means of AFM. The dashed line is a linear fit, indicating that the average nanocrystal consists of 7.62×10^4 gold atoms.

On the basis of a simple calculation, considering the average particle radius $r = 6.6$ nm and assuming that all gold ions in solution are consumed in the formation of the colloids, we find that the number density of particles in suspension amounts to $N = 7.70 \times 10^{18}$ m^{-3}.

Substrates. Polished silicon wafers with a 2.2 nm native oxide are cleaved into 12×12 mm^2 pieces. Prior to handling, these substrates are cleaned ultrasonically in methanol for at least 15 min. A high surface affinity for the colloidal gold particles is achieved by derivatization of the silicon substrates in a 10% (3-aminopropyl)triethoxysilane (APTES) in methanol solution for 60 min, followed by thorough rinsing in methanol. After drying in a nitrogen flow, the samples are immersed in water for 15 min. Deposition of the gold particles is done by immersion in the colloidal suspension, typically for a few hours; underivatized samples do not show any deposition of gold on the surface.

Optical Characterization. Optical extinction spectra are obtained with an HP8452-A UV/vis spectrophotometer. The optical path of the cuvette is $\ell = 10^{-2}$ m. For the optical characterization of substrates without and with adsorbed colloidal films, we used a home-built rotating polarizer spectroscopic ellipsometer equipped with a Xe lamp and a scanning monochromator.[24] Measurements are preformed, both in situ during deposition and ex situ after deposition, in the visible region of the spectrum at wavelengths between 300 and 800 nm at a fixed incident angle of 70°. In situ measurements during colloid deposition are performed in a PTFE (Teflon) cell; absorption of light in the cell windows (standard BK7 glass) and the aqueous solution imposes a lower wavelength limit of approximately 350 nm. Both the incoming and outgoing light beams pass perpendicular to the cell windows; no measurable effects related to transmission through the BK7 glass windows have been observed.

Surface Characterization. Atomic force microscopy (AFM) images are obtained using a Molecular Imaging PicoSPM system, operated in AAC mode or MAC mode,[36] employing silicon cantilevers with a typical resonance frequency of 65 kHz (Nanosensors); for MAC mode, magnetically coated (Molecular Imaging) cantilevers are used. As the tip radius is of the order of 10 nm, the gold colloids appear considerably larger than their actual size because of convolution of tip and particle shapes. Fractional surface coverages φ are determined by counting the number of colloids in a particular area and multiplying by πr^2 with $r = 6.6$ nm the average particle radius.

X-ray fluorescence measurements are performed employing an XRF 2400 Cr-spectrometer with a spot diameter of 10 mm. The calculated density of gold atoms was not sensitive to variation of the assumed thickness of the citrate layer on the particle surface.

Single-Particle Characterization

An accurate, quantitative optical characterization of thin colloidal gold films is only possible if the dielectric function of the individual particles is known. Owing to
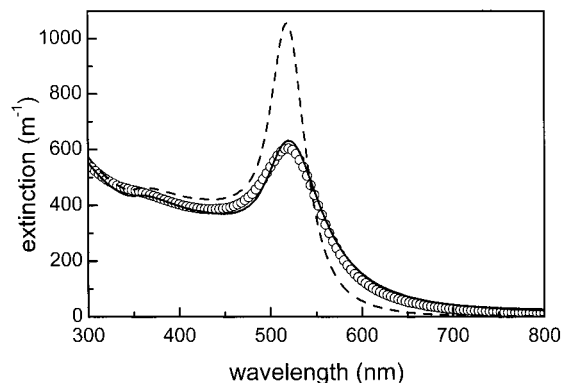

Figure 2. Wavelength-dependent extinction coefficient of an as-prepared colloidal solution, obtained from a measured absorbance spectrum.[37] Calculated extinction coefficients using bulk (dashed line) and modified (solid line) dielectric functions are also shown.

their small size, the optical properties of nanocrystals are markedly different from those of bulk material. Therefore, we first study the optical properties of single colloidal particles in suspension by means of optical absorbance spectroscopy. The extinction coefficient σ_{ext} of our as-prepared colloidal gold suspension, calculated from absorbance measurements,[37] is shown in Figure 2 as a function of wavelength. The maximum at 519 nm, often referred to as the surface plasmon resonance, results in a pink color of the suspension, in good agreement with previous work. Upon dilution of the suspension, the entire extinction spectrum scales linearly with the particle concentration. Apparently, the extinction is dominated by absorption (which is proportional to the particle number density), and scattering can be neglected, as expected for particles much smaller than the wavelength of the light.[38]

The response of spherical particles in a colloidal suspension to an electromagnetic field can be calculated exactly using Mie theory. However, as the particles are much smaller than the wavelength, the optical properties can be analyzed in the quasi-static regime (also referred to as the Rayleigh regime). In this approximation ($r \ll \lambda$), the extinction cross section is due to dipolar absorption only; the scattering cross section and higher multipolar contributions (such as quadrupole extinction and scattering) are strongly suppressed in this size regime.[30] The extinction coefficient in the quasi-static approximation is given by

$$\sigma_{\text{ext}} = \frac{2\pi\sqrt{\epsilon_1}N}{\epsilon_0\lambda}\text{Im}(\alpha) \tag{10}$$

with N the particle number density, λ the wavelength of the light, and ϵ_1 the dielectric function of the medium in which the colloids are suspended. The single-particle polarizability α is related to the dielectric function through the Clausius–Mosotti relation:

$$\alpha = 3\epsilon_1\epsilon_0 V\frac{\epsilon - \epsilon_1}{\epsilon + 2\epsilon_1} \tag{11}$$

(36) Han, W.; Lindsay, S. M.; Jing, T. *Appl. Phys. Lett.* **1996**, *69*, 4111–4113.

(37) The extinction coefficient σ_{ext}, defined by $I/I_0 = \exp(-\sigma_{\text{ext}}z)$ with I/I_0 the attenuation of the light intensity at depth z in the suspension, is determined from the optical absorbance A given by $A = -\log I/I_0$, using the known optical path length $\ell = 10^{-2}$ m.

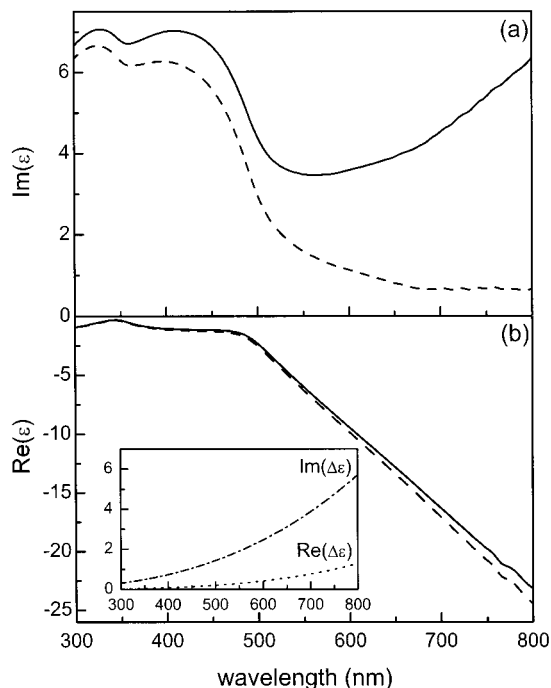(38) van Hulst, H. C. *Light scattering by small particles*; Dover Publications: New York, 1981.

Figure 3. (a) Imaginary and (b) real parts of the complex dielectric function of gold. The dashed lines refer to bulk values,[40] while the solid lines depict the modified dielectric function, as described in the text. The inset shows the wavelength-dependent corrections $\Delta\epsilon_1$ and $\Delta\epsilon_2$ of the real and imaginary parts, respectively.

where $V = {}^4/_3\pi r^3$ is the particle volume, $\epsilon_0 = 8.85 \times 10^{-12}$ F/m is the permittivity of vacuum, and ϵ is the complex dielectric function of the particle. The bulk dielectric function for gold[40,39] is shown in Figure 3 by the dashed lines. In Figure 2 the dashed line shows the calculated extinction using the aforementioned bulk optical properties of gold. Qualitatively, the features of the measured spectrum are reproduced. The extinction maxima are at the same wavelength, but the calculated peak is considerably higher and markedly narrower. Nevertheless, the difference between measured and calculated extinction is negligible on the small-wavelength side of the spectrum. A similar decrease of the height and broadening of the peak for gold nanocrystals with a size below approximately 30 nm has been observed.[14] Surprisingly, however, these spectra are often only compared qualitatively, and merely the position of the surface plasmon resonance is considered.

The differences between calculated and measured extinction can be accounted for by considering the limited electron mean free path due to the small particle size.[30,41] Within the classical electrical conductivity theory, the overall relaxation frequency for bulk material $\Gamma_\infty = \sum\Gamma_i$ is composed of contributions Γ_i due to interactions with phonons, electrons, impurities, and lattice defects. Assuming that only electrons near the Fermi surface (with Fermi velocity v_F) contribute to the conductivity, the mean free path ℓ_∞ is related to Γ_∞ through $\Gamma_\infty = v_F/\ell_\infty$. For gold ℓ_∞ amounts to 42 nm. As our colloidal particles are markedly smaller than this, the effective mean free path is reduced considerably. Following Matthiessen's rule, the additional

scattering of conduction electrons gives rise to an extra term in the relaxation frequency

$$\Gamma(r) = \Gamma_\infty + A\frac{v_F}{r} \tag{12}$$

in which $A = {}^4/_3$ is a theory-related constant. This size-dependent relaxation frequency leads to an alteration of the dielectric function $\epsilon(\lambda,r) = \epsilon_{bulk}(\lambda) + \Delta\epsilon(\lambda,r)$, which, in turn, now also becomes size-dependent. The correction $\Delta\epsilon(\lambda,r)$ of the dielectric function due to intrinsic size effects can be expressed in terms of the difference of two Drude expressions:[41]

$$\Delta\epsilon = \frac{\omega_p^2}{\omega}\left(\frac{1}{\omega + i\Gamma_\infty} - \frac{1}{\omega + i\Gamma(r)}\right) \tag{13}$$

where $\omega = 2\pi c/\lambda$, with c the speed of light. As this simple model only takes into account free electron effects, the correction is largest at longer wavelengths.

With the size-dependency of the dielectric function $\epsilon(\lambda,r)$, and thus the polarizability α, we are able to calculate the modified extinction employing eqs 10 and 11. The plasma frequency ω_p and the Fermi velocity v_F are not known for these small particles. With the bulk values $\omega_p = 8.8$ eV and $v_F = 1.39 \times 10^6$ m/s, the best fit upon varying r (shown by the solid line in Figure 2) yields the particle radius $r = 4.2$ nm. This value is much lower than the physical nanocrystal radius 6.6 nm. Several reasons for this discrepancy can be envisaged. First of all, the TEM images reveal that the gold nanoparticles generally consist of multiple crystalline domains. This enhances scattering of electrons and decreases the electron mean free path even further, compared to the bulk value. Furthermore, the radius obtained by fitting is very sensitive to ω_p and v_F, the exact values of which are not known for these small particles. The shift of the surface plasmon resonance of nanocolloidal gold suspensions with varying dielectric constant of the solvent[42] yields the plasma frequency $\omega_p = 9.9$ eV. The best fit with this value inserted into eq 12 yields $r = 5.3$ nm. The sensitivity to the precise value of v_F is comparible.

The modified dielectric functions are shown in Figure 3 by the solid lines; the inset depicts the corrections Re($\Delta\epsilon$) and Im($\Delta\epsilon$) of the real and imaginary parts, respectively. As mentioned above, the correction is largest at longer wavelengths and much more pronounced for Im(ϵ). The calculated extinction coefficient using this modified dielectric function yields a broader, but also lower peak. At longer wavelengths, between 550 and 800 nm, the tail of the extinction is much higher compared to what is calculated using the bulk dielectric function, in agreement with experimental observations.

Finally, we also attempted to determine the dielectric function from the extinction using a Kramers−Kronig (K−K) transformation. The extinction measurement together with the inverse of eq 10 provides the imaginary part of the particle polarizability. As the imaginary and real parts of the polarizability are K−K consistent, the real part can be calculated. However, as the extinction is measured over a limited wavelength range and extrapolation of the spectrum is not obvious, especially at short wavelengths, the K−K transformation does not yield accurate results, especially at the edges of the spectral range. Qualitatively, results similar to those shown in Figure 3 are obtained.

(39) Johnson, P. B.; Christy, R. W. *Phys. Rev. B* **1972**, *6*, 4370−4379.

(40) The bulk dielectric function of gold was determined using spectroscopic ellipsometry on a 1.5 μm thick gold film on mica. The results are in agreement with literature data.[39]

(41) Klebtsov, N. G.; Bogatyrev, V. A.; Dykman, L. A.; Mel'nikov, A. G. *Opt. Spectrosc.* **1996**, *80*, 113−121.

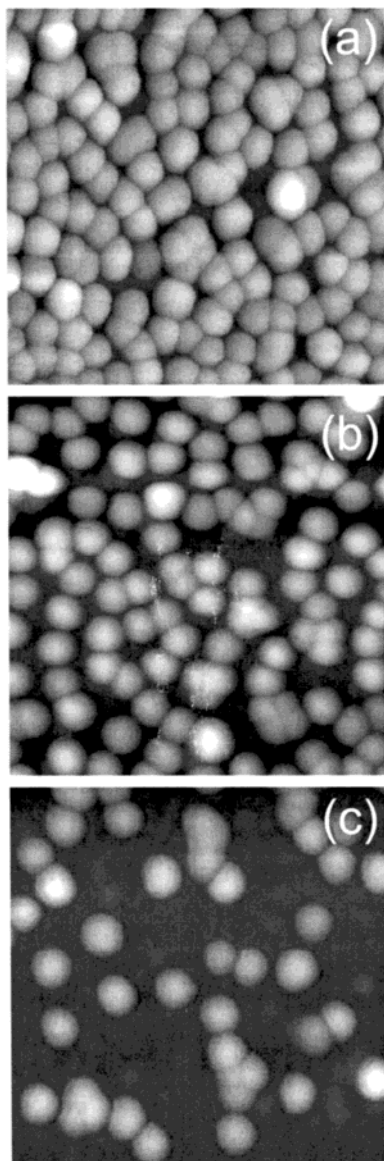(42) Mulvaney, P. *Langmuir* **1996**, *12*, 788−800.

Figure 4. AFM images of three samples with different coverages of gold colloids. The fractional surface coverages φ, determined by counting the particles, amount to 24.7% (a), 13.9% (b), and 6.1% (c). The scan size in all images is 300 nm $\times$ 300 nm.

In the next part of this paper, we will only use the modified dielectric functions, as shown in Figure 3 by the solid lines, to describe the optical properties of our colloidal particles.

Ex Situ Characterization of Colloidal Assemblies

In Figure 4 AFM images for different fractional coverages φ are shown. Tuning of the surface coverage of gold colloids on the silicon/silicon oxide substrate can be achieved by varying the immersion time of the substrates in the colloidal suspension or by changing the ionic strength of the solution by adding inert ions to the solution. Of these two methods, the former has the problem that often inhomogeneous distributions of particles on the surface are observed. Owing to the relatively small scan size, this often hinders accurate determination of the surface coverage by AFM measurements. The second method for varying the amount of adsorbed colloids is demonstrated in Figure 5, where the final surface coverage is plotted as a function of the ionic strength $\frac{1}{2}\sum_i z_i^2 c_i$ of the
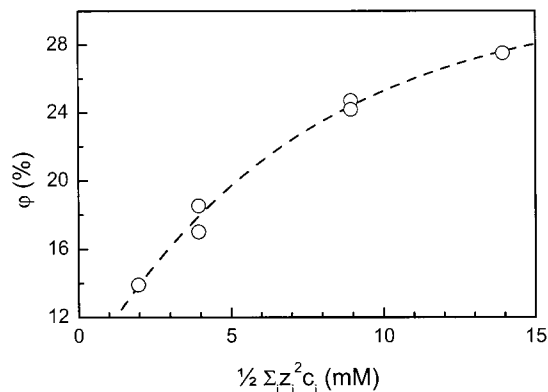

Figure 5. Surface coverage φ, determined from AFM images, as a function of the ionic strength of the colloidal suspension from which the gold particles are deposited. The ionic strength is varied by adding NaCl. The dashed line is a guide for the eye.

solution. The summation is over all ions i in solution where z_i and c_i are their valences and concentrations, respectively. With increasing ionic strength, the Debye length, which describes the extent of the repulsive interaction between the like-charged particles, decreases. This leads to a smaller effective radius of the particles, giving rise to higher surface coverages. The influence of ionic strength on the colloid deposition process will be described in detail elsewhere.[43]

In the AFM images in Figure 4, the colloids appear as spherical particles with a diameter of approximately 30 nm. As described earlier in the Experimental Section, convolution of the tip (radius $\approx$ 10 nm) and the particle (radius $\approx$ 6.6 nm) leads to an enlargement. Moreover, as is seen most clearly for the highest coverage in Figure 4a, the center-to-center distance between particles can be smaller than the apparent diameter, also indicating that the particle images are convoluted. The vertical scale in the images indicates a height of 13.2 nm, which is in agreement with the particle size as determined from TEM measurements. In Figure 1 the linear relation between the number of gold atoms, determined from X-ray fluorescence measurements, and the colloid density, obtained from AFM images on the same samples, over a significant range of surface coverages indicates that AFM provides a representative means to probe the absolute surface coverage.

Figure 6 shows ellipsometry spectra of samples before and after gold colloid deposition. After immersion in the suspension (typically for 10 h), the samples are dried in a nitrogen gas flow. The spectra of the bare silicon/silicon oxide substrate are in good agreement with a model calculation using a three-layer model and the known thickness of the silicon oxide layer. The deposition of colloidal gold particles has a marked effect on the ellipsometry measurements. As expected for a thin layer of deposited material, the change in cos Δ is much more pronounced than the change in tan Ψ. Apart from an upward shift in cos Δ over the entire wavelength range, a characteristic peak develops with increasing numbers of gold particles on the surface. The position of the peak maximum near 520 nm corresponds to the surface plasmon resonance of the gold colloids (see Figure 2). The tan Ψ spectra at short wavelengths show a slight decrease with respect to the bare substrate spectrum, independent of surface coverage. At the wavelength where cos Δ exhibits a maximum, an increase in tan Ψ is observed.

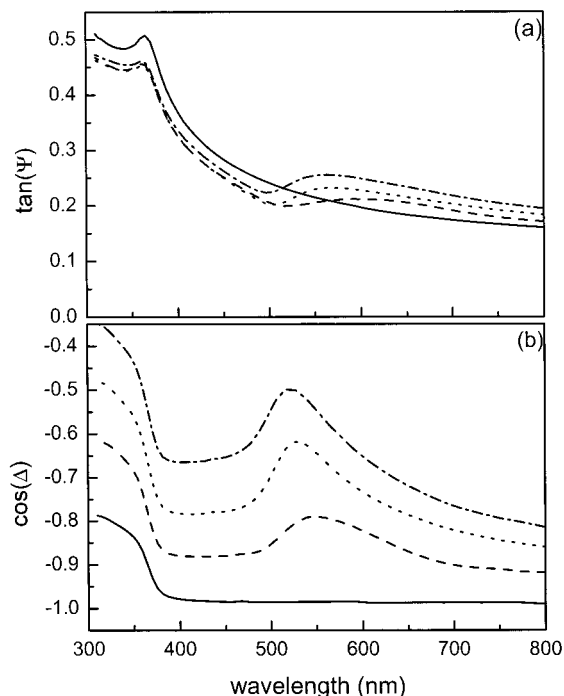(43) Kooij, E. S.; Brouwer, E. A. M.; Wormeester, H.; Poelsema, B. Unpublished.

Figure 6. Ellipsometry spectra for (dry) samples with different gold colloid coverages, measured in air. The solid lines represent the spectrum of a bare silicon/silicon oxide substrate (for which $\varphi = 0$), while the broken lines correspond to samples for which the AFM images are shown in Figure 4. The coverages are $\varphi = 6.1\%$ (dashed lines), $\varphi = 13.9\%$ (dotted lines), and $\varphi = 24.7\%$ (dash−dotted line).
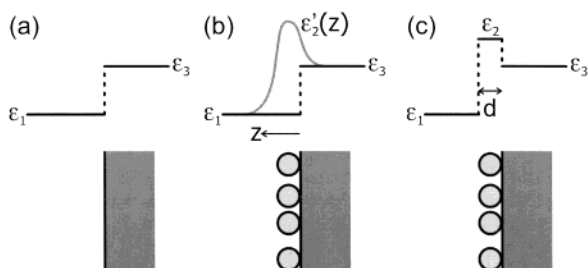

Figure 7. Schematic representation of dielectric function profile across the ambient−substrate interface. For the bare substrate (a) a simple step profile is used, while upon absorption of colloidal particles (b) a coverage-dependent correction ϵ_2 is added. In the most simple approximation, ϵ_2 is constant over the colloidal film thickness, yielding a two-step profile (c).

Optical Invariant Analysis

Analysis of our ellipsometry spectra, independent of an optical model, can be performed in terms of optical invariants.[44] In the thin film approach ($d \ll \lambda$), the dielectric profile across the ambient−substrate interface is described as a step profile, plus a small correction which depends on the surface coverage of colloidal particles. This is schematically illustrated in Figure 7. By treating inhomogeneities at the surface as perturbations, the change in the dielectric profile upon adsorption of colloidal particles can in a first approximation be described by

$$\frac{\rho_{1234}}{\rho_{134}} - 1 = \eta J \qquad (14)$$

where ρ_{1234} and ρ_{134} are the complex reflection coefficients

(44) Lekner, J. *Theory of reflection*; Martinus Nijhoff Publishers: Dordrecht, 1987.

(eq 1) for a silicon/silicon oxide substrate with and without a colloidal gold layer, respectively. The prefactor η represents an energy-dependent but thin-film-independent constant, while the optical invariant J describes the thin film. In principle, the contribution of the oxide layer can be neglected, as we can rewrite

$$\frac{\rho_{1234}}{\rho_{134}} = \frac{\rho_{1234}}{\rho_{14}} \bigg/ \frac{\rho_{134}}{\rho_{14}} = \frac{1 + \eta(J_{ox} + J_{Au})}{1 + \eta J_{ox}} = 1 + \frac{\eta J_{Au}}{1 + \eta J_{ox}} \qquad (15)$$

where J_{ox} and J_{Au} represent the contributions from the oxide and the colloidal gold layer, respectively. In the limit of thin films (which is the case for both the oxide layer and the layer of colloidal particles), $\eta J_{Au} \ll 1$ and $\eta J_{ox} \ll 1$, so $\eta^2 J_{Au} J_{ox}$ is negligible, and we can in first-order neglect the contribution from the oxide to the optical invariant and take

$$\frac{\rho_{1234}}{\rho_{134}} = 1 + \eta J_{Au} \qquad (16)$$

As is clear from the above, the prefactor η is independent of the thin films and is given by

$$\eta = i \frac{4\pi e}{\lambda} \frac{\sqrt{\epsilon_1} \cos(\theta)}{\epsilon_1 - \epsilon_4} \frac{\epsilon_4 \sin^2(\theta)}{\epsilon_4 \cos^2(\theta) - \epsilon_1 \sin^2(\theta)} \qquad (17)$$

with λ the wavelength (in meters) and e the electron charge. This prefactor only depends on the angle of incidence θ and the dielectric functions ϵ_1 and ϵ_4 of the ambient and substrate, respectively. The optical invariant J is related to the dielectric properties of the colloidal layer through

$$J = \int_{-\infty}^{\infty} dz \frac{(\epsilon_1 - \epsilon_2'(z))(\epsilon_2'(z) - \epsilon_4)}{\epsilon_2'(z)} \qquad (18)$$

where $\epsilon_2'(z)$ is the height-dependent dielectric function of the adsorbed layer (see Figure 7b).

Without specifiying the dielectric profile across the interface, we can qualitatively analyze spectra like those in Figure 6 using a principal component analysis (PCA).[31] A PCA is employed to represent the original ellipsometry spectra by a set of orthogonal spectra, the principal components. The product of two of these components is zero. Superposition of the components, weighted with coefficients C_i, again produces the original spectra. If these original ellipsometry spectra have common features, most of the orthogonal components merely represent noise. Details of the application of PCA to our system and the calculations involved will be described elsewhere.[45]

To perform a PCA, we first calculate the quantity on the left of eq 14 for every sample by taking the spectra after deposition and of a bare substrate (ρ_{1234} and ρ_{134} correspond to the broken and solid lines in Figure 6, respectively). Note that as the spectra are complex quantities, so are the coefficients C_i. Including samples with different coverages (determined from AFM images), we find that the first component is predominant and with only the coefficient C_0 our results are adequately described; the contribution of all other components together amounts to less than 3% for all spectra used in the calculation. As particle−particle interactions are expected to depend on the actual coverage, this seems to indicate that the

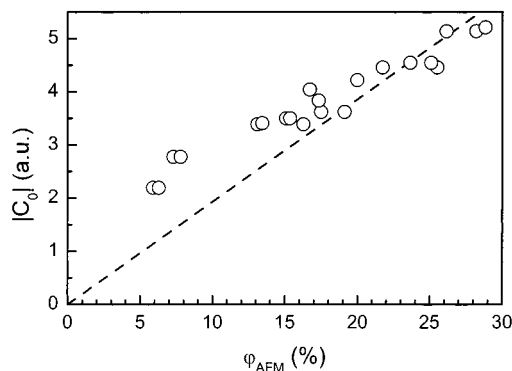(45) Brouwer, E. A. M.; Kooij, E. S.; Wormeester, H.; Poelsema, B. Unpublished.

Figure 8. Result of a principal component analysis on spectra like those in Figure 6. The absolute value of the coefficient C_0 for the dominant first component is plotted as a function of the fractional surface coverage φ_{AFM} as determined from AFM measurements. The dashed line is a linear fit through the origin to the data points for which $\varphi_{AFM} > 20\%$.

adsorbed colloids behave as individual entities on the surface. Also, it appears reasonable to assume that the value of the coefficient is in some way related to the particle density on the surface. In Figure 8 the absolute value of the first coefficient $|C_0|$ is plotted as a function of the fractional surface coverage φ_{AFM} determined from AFM images such as those in Figure 4. Assuming that $|C_0|$ indeed is related to the surface particle density, in a first approximation all data points are expected to lie on a linear fit through the origin. The dashed line shows that this is approximately the case for the coverages above 15–20% but that at lower coverages a higher value for $|C_0|$ is obtained. This deviation from the linear relationship will be discussed in a later section.

Quantitative Interpretation of the Invariant

A more quantitative approach is possible when, in a simple approximation, we consider a constant dielectric function ϵ_2 over the whole layer thickness d. In this case the dieletric profile is a two-step function (see Figure 7c), and eq 18 reduces to

$$J = d(\epsilon_1 - \epsilon_2 + \epsilon_4 - \epsilon_1\epsilon_4/\epsilon_2) \tag{19}$$

For spectra corresponding to different coverages, the invariant J can be calculated using eq 14. As discussed in the previous section, we can in principle neglect the thin oxide layer. However, the results presented in the following were considerably improved by not just using the silicon dielectric function for ϵ_4 in eq 17 but also replacing it with a pseudo-dielectric function ϵ_4^* determined from the ellipsometry spectra of the oxidized substrate.[46] This improvement can be rationalized, as it has been shown that deviations introduced by using the invariant approximation become pronounced even for thicknesses as small as 5% of the wavelength of the light.[47]

We can now solve J in eq 19 for ϵ_2, and this generally yields two solutions. However, as the optical absorption cannot be negative, only the results for which $\text{Im}(\epsilon_2) \geq 0$ are physically correct. Additionally, we need to specify a thickness d in eq 19. Although the particles are 13.2 nm, the extent of the dielectric function seems to be larger, as good results with $\text{Im}(\epsilon_2) \geq 0$ and no singularities were only obtained with thicknesses above 25 nm; this markedly
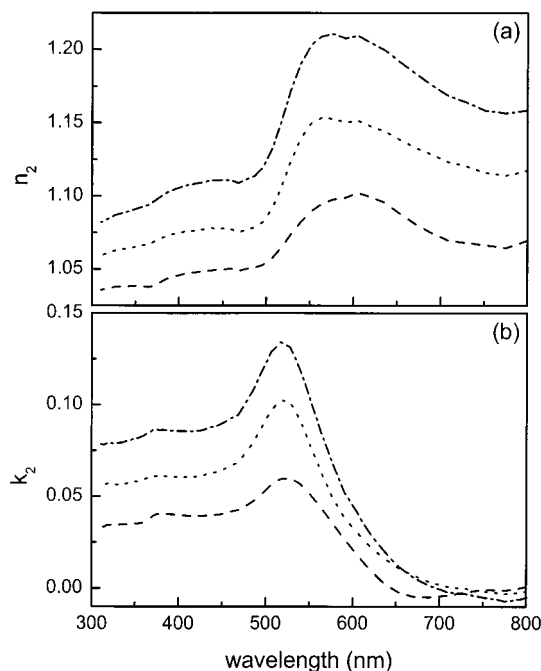
(46) The pseudo-dielectric function ϵ_4^* of a bulk material with a thin layer $(d \ll \lambda)$[22] can be estimated by treating it as a two-layer system.
(47) McIntyre, J. D. E.; Aspnes, D. E. *Surf. Sci.* **1971**, *24*, 417–434.

Figure 9. Real (a) and imaginary (b) part of the complex refractive index for colloidal gold films of different coverages, determined using the optical invariant as described in the text. The coverages are the same as those of Figure 6.

larger thickness in comparison to the particle radius will be discussed in a later section. From the determined dielectric function ϵ_2 we can directly determine the complex index of refraction $n_2 + ik_2 = \epsilon_2^{1/2}$. The real and imaginary parts n_2 and k_2, as determined from the ellipsometric spectra in Figure 6, are shown in parts a and b, respectively, of Figure 9.

In the absence of significant scattering, as is the case for these small particles, and neglecting the interparticle interaction, the extinction is linearly dependent on the surface particle density. The extinction of the colloidal films can be calculated from the imaginary part of the refractive index via $\sigma_{ext} = 4\pi k_2/\lambda$, yielding the broken lines in Figure 10a. We can compare this to calculations for single particles suspended in air obtained from eqs 10 and 11 and by using the density N as a fitting parameter. The solid lines in Figure 10a were obtained using $N = 1.04 \times 10^{23}$ m^{-3}, $N = 0.79 \times 10^{23}$ m^{-3}, and $N = 0.46 \times 10^{23}$ m^{-3}. Similar characteristic features are observed in the extinction spectra determined using the invariant and those calculated using eqs 10 and 11. However, the peak corresponding to the surface plasmon resonance is red-shifted and somewhat broader in the "invariant" extinction, which is most pronounced for the lowest coverages. From the fitted surface density N, the film thickness 25 nm, and the surface area πr^2 per particle, we can calculate the surface coverage φ_{inv}. In Figure 10b φ_{inv} is plotted as a function of the AFM coverage φ_{AFM}. As is clear from the line with slope 1, the coverage determined in this way is in reasonable agreement with that obtained from AFM. At coverages below approximately 20%, the optically derived coverage appears to be overestimated. This will be discussed in a later section.

In Situ Spectroscopic Ellipsometry

The results presented and analyzed in the previous sections all pertain to ex situ measurements. In this section we present in situ spectroscopic ellipsometry results and compare them to the ex situ experiments. In Figure 11
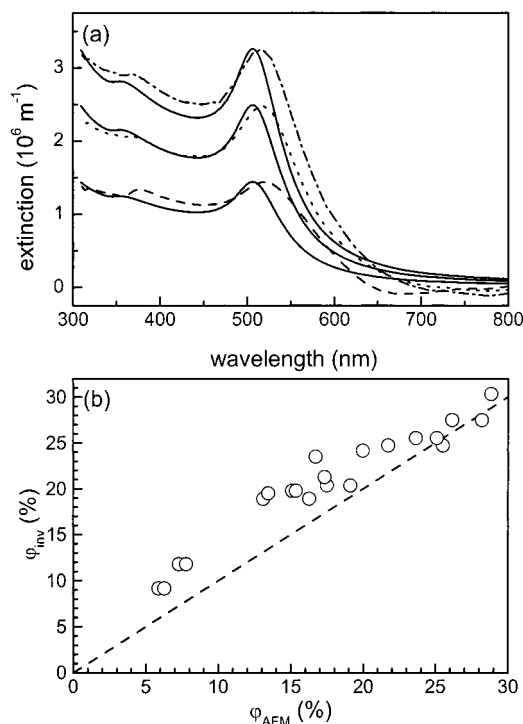
Figure 10. (a) Extinction coefficients determined from k_2 in Figure 9 (broken lines) compared to calculations for gold particles in air using eqs 10 and 11 with the modified dielectric function for gold in Figure 3. The particle densities $N = 1.04 \times 10^{23}$ m^{-3}, $N = 0.79 \times 10^{23}$ m^{-3}, and $N = 0.46 \times 10^{23}$ m^{-3} are used in eq 10, corresponding to the surface coverages $\varphi = 24.7\%$, $\varphi = 13.9\%$, and $\varphi = 6.1\%$, respectively. (b) Surface coverage φ_{AFM} determined using the optical invariant as a function of the coverage φ_{AFM} determined from AFM images. The dashed line has a slope of 1.

ellipsometry spectra are shown for a substrate before and after adsorption of colloidal gold in contact with an aqueous environment. The spectrum for a bare substrate (solid lines) is markedly different from that in air (compare Figure 6, solid lines). Although the maximum in tan Ψ near 360 nm is still present, the entire tan Ψ spectrum is shifted to lower values. In contrast, cos Δ is less negative over the entire spectral range and exhibits a strong increase at longer wavelengths. Because of the difference in optical contrast in the case of water or air, the Brewster angle changes,[22] resulting in a shift of the crossover in cos Δ to shorter wavelengths when measuring in water. This effect also leads to a dramatically increased sensitivity for surface modifications at this angle.

After obtaining the bare spectrum (after APTES-treatment), the water is replaced by an aqueous colloidal gold suspension and particles start to adsorb at the surface. This process can be followed in situ. The results of a detailed study of the adsorption kinetics will be described in a separate publication.[45] The adsorption saturates typically in 10 h, after which the gold suspension is removed. The cell is rinsed several times with water before an ellipsometry measurement is performed. The resulting spectra of a gold-covered substrate in water (dashed lines) and air (thin dotted line) are also shown in Figure 11. The overall coverage as determined by AFM (see the inset in Figure 11) amounts to $\varphi = 7.6\%$. In both spectra the peak in cos Δ at 520 nm corresponding to the surface plasmon resonance is clearly observed, but the features of the spectra obtained in water are considerably more pronounced than those in the "dry" spectra. The "dry" and "wet" spectra can be measured reproducibly after repeated rinsing and/or drying, indicating that the particles adhere
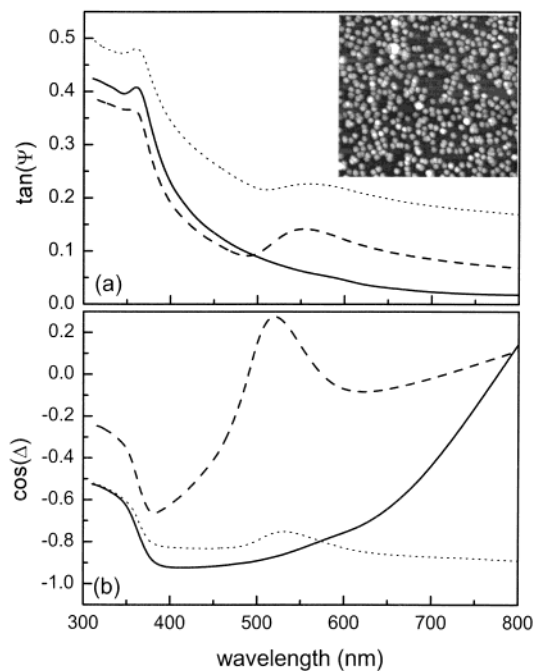

Figure 11. Comparison of ellipsometry spectra measured in aqueous solution (dashed line) and after drying in air (dotted line). The solid line represents the ellipsometry spectrum, obtained in water, for a silicon/silicon dioxide sample without adsorbed gold. The inset shows a 1 μm $\times$ 1 μm AFM image of the sample measured after drying. The coverage amounts to $\varphi = 7.6\%$.

to the substrate surface and are not washed off or reorganize upon drying.

Similar to the analysis of the ex situ ellipsometry experiments in the previous sections, we can also use the optical invariant analysis on these "wet" spectra to determine the coverage of gold particles. For the dielectric function of the ambient, we now use the slightly wavelength-dependent value for water (for the spectral range 300–800 nm, $\epsilon_{H_2O}(\lambda) = 1.759 + 5516/\lambda^2$) instead of $\epsilon_1 = 1$. The dielectric function ϵ_2 of the layer is determined using eq 19, but now we compare it to the extinction of gold particles suspended in water, given by eqs 10 and 11 with $\epsilon_1 = \epsilon_{H_2O}(\lambda)$. This yields the coverage $\varphi_{inv}^{wet} = 11.2\%$, which is only slightly smaller than the value $\varphi_{inv}^{dry} = 11.8\%$ for the dried sample.

Simulations of Ellipsometry Spectra

In the previous sections, we calculated optical invariants from the measured ellipsometry spectra and determined the particle coverage by comparing the extinction of the colloidal film to that calculated for a single particle. Despite the very crude and simple approximation for the dielectric function profile across the interface, this top-down approach yields a surprisingly good estimate of the surface coverage.

An alternative way to obtain quantitative information is to calculate the ellipsometry spectra using a specific model for the system to be analyzed. In this bottom-up approach, the particle surface density can be used as a fitting parameter. The primary question which again interests us is as follows: Is it possible to accurately determine the particle coverage by optical means?

The obvious problem in simulating the optical response of any system is the choice of the dielectric function of an unknown material, the colloidal gold film in our case. Using a homogeneous gold film with a thickness equivalent to
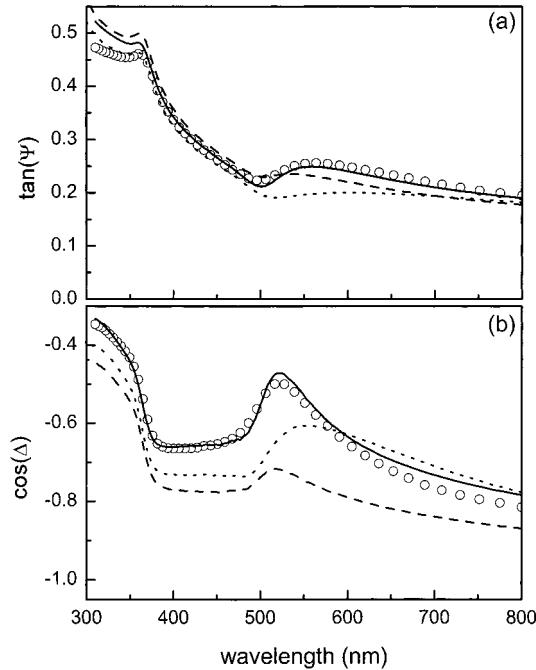
Figure 12. Calculated ellipsometry spectra for a silicon/silicon oxide sample with 24.7% gold coverage. The Bruggeman (dotted lines) and Maxwell−Garnett (dashed lines) effective medium approximations (eq 5) were used to model the dielectric function ϵ_2 of the colloidal film with the fill fraction $f = 0.165$. The solid lines represent a calculation using the thin island film theory, with a surface coverage equal to that obtained with AFM. The open circles represent the ellipsometry data for a film with φ = 24.7% (corresponding to the dash−dotted line in Figure 6).

the amount of colloidal gold yields spectra which are totally different from the measurements.

The dielectric function ϵ_2 of the colloidal layer can be mimicked using an effective medium approximation[30] in combination with the surface coverage φ_{AFM} determined from AFM images. The volume fraction f needed in eq 5 for spherical particles is related to the surface coverage through $\varphi = 1.5f$.[48] With the Abeles matrices in eqs 2 and 3, the optical response of our multilayered sample can be calculated and compared to the experimental spectra. In Figure 12, the experimental ellipsometry result of a colloidal gold film with coverage φ = 24.7% is compared to calculations using the Bruggeman (dotted line) and Maxwell−Garnett (dashed line) effective medium approximations. The thickness 13.2 nm was used for the colloidal film with the volume fraction f = 0.165. In both simulations, considerable differences are observed in comparison to the experimental data. This is most clearly visible in cos Δ. Apart from being much lower, the calculation using the Bruggeman effective medium approximation exhibits a much broader peak in cos Δ, and the features in tan Ψ also extend to markedly longer wavelengths. The Maxwell−Garnett approximation yields a peak in cos Δ which is in qualitative agreement with the experimental result but is much too low. Increasing the volume fraction f (corresponding to a higher coverage) results in an increase in cos Δ, but with both the Bruggeman and the Maxwell−Garnett approximation, the spectra never approach the experimentally obtained results.

Considerably better results are obtained using the thin island film theory developed by Bedeaux and Vlieger.[32,33]

---

(48) In our definition of the surface coverage φ, we consider the particles as disks with the volume $2r\pi r^2$, while the actual volume occupied by the spheres amounts to $^4/_3\pi r^3$.
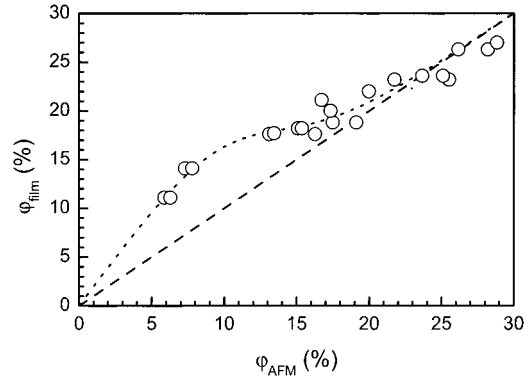

Figure 13. Surface coverage φ_{film}, obtained by fitting the experimental spectra to the thin island film theory, as a function of the coverage φ_{AFM} determined from AFM images. The dashed line has a slope of 1 while the dotted line is a guide for the eye which is discussed in the next section.

The two main features of this theory are that the film under consideration (i) has a small thickness compared to the wavelength of the light and (ii) is discontinuous. As in the previous paragraphs, the optical characteristics of such films are almost always described by an effective dielectric function and an optical thickness. The precise determination of this thickness for optically thin films is often unclear, owing to the strong correlation of the thickness and the refractive index. Bedeaux and Vlieger describe the optical properties of thin island films in terms of excess polarization and magnetization densities, positioned at a certain dividing plane. Usually, this dividing plane is taken to coincide with the physical substrate−ambient interface.

The solid lines in Figure 12 show cos Δ and tan Ψ, calculated using the Abeles matrix for a particulate film in eq 8 and inserting the coverage φ = 24.7% in eq 6. Clearly, the measured features in both cos Δ and tan Ψ are reproduced much better than those with the Bruggeman or Maxwell−Garnett effective medium approximations (dotted and dashed lines, respectively). Note that, as mentioned in a previous section, we used a modified dielectric function for the gold. With the bulk values, a much higher peak in cos Δ is calculated and the agreement between experiment and simulation is considerably worse.

In stead of merely calculating the spectra on the basis of the known surface density of nanocrystals, we can also fit the experimental spectra to the thin island film theory with the coverage φ_{film} as a fitting parameter. The resulting coverages φ_{film} are shown in Figure 13 as a function of the coverage φ_{AFM} determined by AFM. As with the results of the invariant analysis, the dashed line with slope 1 again indicates that the coverage determined by ellipsometry is in good agreement with what is found on the basis of AFM measurements for coverages above approximately 20%. Below 20% coverage, the optical analysis using the thin island film theory also leads to an overestimation.

The coverages obtained by fitting the ellipsometry spectra to the thin island film theory can also be compared to the results of the principal component analysis (PCA) in one of the previous sections. In Figure 14 the absolute value of the first coefficient $|C_0|$, also shown in Figure 8, is plotted as a function of the optically derived coverage φ_{film}. The perfect linear relation between the two over a significant range of fractional surface coverages indicates that the PCA is a reliable and relatively easy way to extract surface coverages from a large amount of spectra. Especially for in situ studies of the growth of thin colloidal
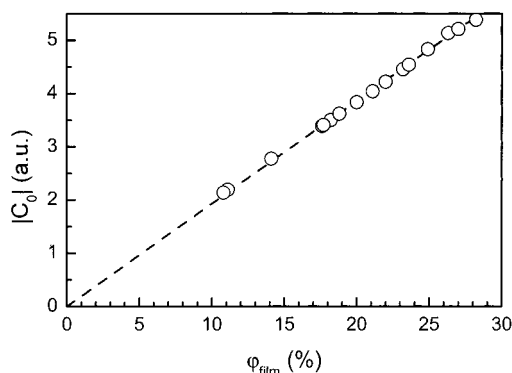
Figure 14. Absolute value $|C_0|$ of the first coefficient from a PCA as a function of the coverage φ_{film} obtained from fitting the ellipsometry spectra to the thin island film theory.

Table 1. Comparison of the Coverages Determined from Ellipsometry Spectra Measured in Air and in Water, Analyzed Using the Optical Invariant Analysis (φ_{inv}) and the Thin Island Film Theory (φ_{film})

	in air ($\epsilon_1 = 1$)	in water ($\epsilon_1 = \epsilon_{H_2O}(\lambda)$)
φ_{AFM}	7.6%	
φ_{inv}	11.8%	11.2%
φ_{film}	14.1%	11.4%

films, this will simplify the analysis considerably.[45] In principle, for a series of measurements, only one single calibration by means of AFM, SEM, or XRF is required.

The above procedure can also be performed on the in situ spectra in Figure 11. Also with these "wet" spectra, the effective medium approximations by Bruggeman and Maxwell–Garnett do not lead to satisfactory results. Again, the theory of thin island films yields better results. The surface coverage determined by fitting the "wet" spectra, $\varphi_{\text{film}}^{\text{wet}} = 11.4\%$, is lower than the value $\varphi_{\text{film}}^{\text{dry}} = 14.1\%$ for the dried sample. The difference is larger than what was found with the invariant analysis; the reason for this difference is unknown. However, the colloid surface density is still markedly higher than the 7.6% obtained from AFM images, as we always find for low coverages. The values for the fractional surface coverages obtained by AFM, the optical invariant method, and the thin island film theory are summarized in Table 1.

Image Charges

The results in Figures 10b and 13 show that the coverages obtained by analysis of the optical spectra are in agreement with what is determined by counting the particles in AFM images. For coverages below approximately 20%, the optical analyses indicate an overestimate of the nanocrystal density on the substrate. In this section, we will discuss the possible effect of image charges and how this may account for this overestimate.

In the investigation of the optical properties of single particles on the basis of extinction measurements on gold suspensions, we argued that the response to an electromagnetic field can be described well by only considering the first electrical dipole contribution (the quasi-static approximation). When the particle is near the substrate, the dipole moment **p** of the nanocrystal will induce an image dipole moment **p′** in the substrate, which is given by

$$\mathbf{p}' = \pm \frac{\epsilon_3 - \epsilon_1}{\epsilon_3 + \epsilon_1}\mathbf{p} \tag{20}$$

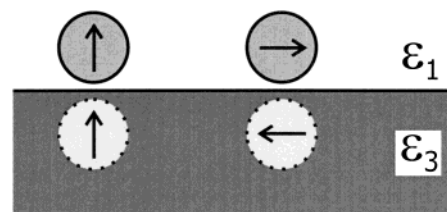where ϵ_1 and ϵ_3 represent the dielectric function of the

Figure 15. Schematic illustration of the image charge effect of a dipole near an interface. The image dipole is oriented parallel to the original dipole when it is normal to the surface. In the case of an orientation parallel to the interface, the dipole and its image are oriented antiparallel.

ambient and the substrate, respectively.[49–51] The sign refers to the orientation of the dipole **p** with respect to the interface, and thus is a function of the polarization state of the incident light. This is schematically illustrated in Figure 15. If the dipole is oriented perpendicular to the substrate, its image will be oriented parallel and the imaged dipole will add to the original dipole moment of the nonadsorbed particle. On the other hand, if the dipole is oriented parallel to the interface, the image will be antiparallel, implying a negative contribution to the overall dipole moment. Note that as the dielectric functions are in principle complex functions, so is the image dipole **p′**. Two extreme cases of eq 20 can be envisaged: (i) $\epsilon_1 = \epsilon_3$ leads to a vanishing image dipole, which is obvious as this condition is equivalent to absence of an (optical) interface; (ii) $|\epsilon_3| \gg |\epsilon_1|$, which in general holds for metals, will lead to an image dipole with identical magnitude, $|\mathbf{p}'| = |\mathbf{p}|$.

The importance of image charge effects is corroborated by several experimental observations in the previous sections. First of all, in the invariant analysis using eq 19, the thickness of the layer d is to be inserted. Physically correct results, that is, with $\text{Im}(\epsilon_2) \geq 0$, were only obtained for thicknesses above approximately 25 nm. A monolayer of nanocrystals has the thickness $2r = 13.2$ nm, but including the contribution of image charges, an increase by a factor of approximately 2 is to be expected. In this simple comparison, we have neglected the presence of the oxide layer. However, the oxide layer thickness of 2 nm is comparible to the size variation of the colloidal particles. Second, the extinction coefficients in Figure 10a, calculated from the refractive index in Figure 9, exhibit a peak which is markedly shifted to longer wavelengths in comparison to that for a single particle. Using a simple calculation, Kreibig showed that the electromagnetic interaction of two particles in a cluster pair leads to a red-shift of the surface plasmon resonance with respect to that of the isolated particles.[30] The shift and broadening of the surface plasmon resonance peak obviously depend on the pair distance. For two touching gold particles, the red-shift amounts to approximately 25 nm. If we consider our adsorbed nanocrystal and its image as a pair of dipole oscillators, this is in reasonable agreement with the difference we observe in the results of Figure 10. Moreover, the shift is the same for all coverages except for the lowest, for which it appears to be slightly larger.

It is difficult to incorporate the effect of image charges on the spectra in Figure 12, calculated using the Maxwell–Garnett and Bruggeman effective medium approximations. In these approximations, the optical response of the particles is described by a single polarizability. As

(49) Yamaguchi, T.; Yoshida, S.; Kinbara, A. *Thin Solid Films* **1974**, *21*, 173–187.
(50) Dignam, M. J.; Fedyk, J. *J. Phys. (Paris)* **1977**, *38*, C557–C565.
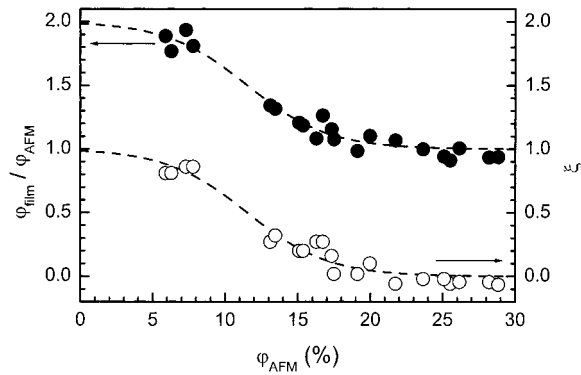(51) Ruppin, R. *Phys. Rev. B* **1992**, *45*, 11209.

Figure 16. (Solid symbols) ratio of the surface coverages φ_{film} and φ_{AFM}, determined by fitting to the thin island film theory and from AFM images, respectively, as a function of the AFM coverage. (Open symbols) proportionality constant ξ as a function of the AFM coverage φ_{AFM}. The values for ξ were determined by fitting the ellipsometry spectra to the thin island film theory, with ξ as the fit parameter. The dashed lines are a guide for the eye.

mentioned above, the orientation of the image dipole and thus the extent of its contribution are strongly dependent on whether the dipole is normal or parallel to the surface. This problem does not arise with the thin island film theory, as it makes use of the two polarizabilities γ and β in eqs 6 and 7, which refer to orientations along and normal to the substrate surface, respectively. In a very simple and crude calculation, we can modify these polarizabilities to include the image charges

$$\gamma' = \left(1 - \xi\frac{|\mathbf{p}'|}{|\mathbf{p}|}\right)\gamma \tag{21}$$

$$\beta' = \left(1 + \xi\frac{|\mathbf{p}'|}{|\mathbf{p}|}\right)\beta \tag{22}$$

As discussed above, the image charge contribution along the surface is negative while orientation normal to the substrate results in an increase of the polarizability.

The quantity ξ is a proportionality constant which describes the extent of the image charge effect. For single, isolated adsorbed nanocrystals, which do not mutually interact, the influence of image charges is maximal and the value $\xi \approx 1$ is expected. However, with increasing surface coverages φ, the value ξ is likely to decrease as a result of depolarization by neighboring nanocrystals. Obviously, in the limit of a continuous layer, image charge effects do not play a role and $\xi = 0$. To get a feeling for the magnitude of the image charge effects, we plot the ratio $\varphi_{film}/\varphi_{AFM}$ of the coverages determined optically and by AFM, respectively, as a function of the actual surface density obtained from AFM images. The result is shown in Figure 16 by the solid symbols, while the dashed line is a guide for the eye. Apparently, the overestimate of the surface density decreases from a factor of 2 at the lowest coverages to 1 at coverages above approximately 20%. The dashed line in Figure 16 is also transferred to Figure 13, representing the coverage as a function of the AFM coverage φ_{AFM}.

The value ξ can be determined with the thin island film theory we used earlier to simulate the ellipsometry spectra. Instead of the polarizabilities in eq 6 we now use the modified values γ' and β' given by eqs 21 and 22. In contrast to the previous section in which we used the surface coverage φ as fitting parameter, we now insert the value φ_{AFM} obtained from AFM images and use the proportion-

ality constant ξ as the fitting parameter. The resulting values for ξ are plotted in Figure 16 (open symbols) as a function of the surface coverage φ_{AFM}. Similar to the ratio $\varphi_{film}/\varphi_{AFM}$, ξ decreases with increasing surface coverage. Note that the absolute values of both $\varphi_{film}/\varphi_{AFM}$ and ξ depend markedly on the actual particle radius inserted into the aforementioned models. In general, a smaller radius leads to an upshift of both quantities in Figure 16.

The decrease of both $\varphi_{film}/\varphi_{AFM}$ and ξ implies that the particle–particle interaction leads to depolarization with decreasing interparticle distances. This is in qualitative agreement with the above. However, it is surprising that the depolarization already becomes very efficient at relatively low surface coverages. Moreover, the film thickness inserted in eq 19 with the invariant analysis does not decrease markedly with increasing coverage. And finally, the aforementioned shift of the extinction spectra in Figure 10 does not vanish at high nanocrystal densities on the surface. It is likely that a description of the precise quantitative features requires an extensive model, which also takes local field effects due to the entire particle assembly and their images into account.

Conclusions

We have presented a detailed study of the optical properties of colloidal gold films assembled on naturally oxidized silicon treated with APTES. Knowledge of both the single particle diameter and its polarizability is a prerequisite for a quantitative analysis of the surface coverage in situ or ex situ with ellipsometry. The diameter of the particle is usually determined from TEM, although AFM or a combination of AFM and XRF provides useful alternatives.

Crystalline metal colloids with grains that are smaller than the electron effective mean free path have optical properties different from those of the bulk material. Especially at long wavelengths, differences between the colloid response and the bulk optical response cannot be neglected. The standard experimental procedure of an absorbance measurement provides an experimentally determined extinction coefficient. This can function as a bench mark for the modification of the bulk dielectric function that takes the limited electron mean free path into account.

The standard analysis procedure of ellipsometric spectra of samples, such as our gold nanocrystal-on-silicon assemblies, involves an effective medium approximation for the dielectric function of the adsorbed colloid layer. Both the commonly used Maxwell–Garnett and Bruggeman approaches, however, lead to highly inaccurate results. We have shown two approaches that both give quantitatively accurate results. The first approach involves the treatment of the colloid layer as a small perturbation and derives a so-called ellipsometric invariant from the spectrum that incorporates in the simplest way the properties of the nanocrystal layer. Without any knowledge of colloid diameter or polarizability, a principal component analysis approach allows a quick quantitative characterization of the coverage. Only a calibration of the coverage is required for the gold colloids studied in this work. A great advantage of this method is that it directly identifies complications in the analysis such as contributions from particle–particle interaction or coalescence with increasing deposition. The ellipsometric invariant can also be used to calculate the extinction of the deposited colloid layer, although this involves a certain model of the deposition geometry. The comparison of the extinction of

the colloid layer with the single particle extinction measured from absorbance measurements provides the number of adsorbed colloids. This number is in excellent agreement with the number obtained from AFM measurements.

The thin island film theory developed by Bedaux and Vlieger, which treats the deposited colloids as excess polarizabilities, allows an accurate calculation of the optical properties. This approach to analyze spectra is necessary if the colloids are deposited on top of a stack of thin films. In such cases the invariant determination will not be appropriate.

All the optical analysis methods show an excellent agreement between the optically determined coverage and the AFM determined coverage above 20% coverage. Below this value, up to a twice-higher coverage is consistently measured optically. An explanation for this is sought in terms of image charges whose influence is coverage dependent.